Device physics of all-polymer solar cells

Mandoc, Maria Magdalena

5

Origin of the reduced fill factor and photocurrent in MDMO-PPV:PCNEPV all-polymer solar cells*

The photogeneration mechanism in blends of MDMO-PPV and PCNEPV is investigated. The photocurrent in the MDMO-PPV:PCNEPV blends is strongly dependent on the applied voltage as a result of a low dissociation efficiency of the bound electron-hole pairs. The dissociation efficiency is limited by the low carrier mobilities, low dielectric constant and the strong intermixing of the polymers, leading to a low fill factor and a reduced photocurrent at operating conditions. Additionally, electrons trapped in the PCNEPV phase recombine with the mobile holes in MDMO-PPV phase at the interface between the two polymers, thereby affecting the open-circuit voltage and increasing the recombination losses. At an intensity of one sun, Langevin recombination of mobile carriers dominates over the trap-assisted recombination.

*Published as: M. M. Mandoc, W. Veurman, L. J. A. Koster, B. de Boer, P. W. M. Blom, Adv. Funct. Mater. **17**, 2167 (2007).

5.1 Introduction

The efficiency of polymer-based solar cells has been increased significantly in the last years. In blends of regioregular poly(3-hexylthiophene) (P3HT) and PCBM, forming bulk heterojunctions, efficiencies of more than 4% have been reported [1-3]. A disadvantage of this type of cells is that one of the components, namely PCBM, only weakly absorbs the visible part of the solar spectrum and the main light absorption occurs in the polymeric phase of the blend. In this respect, all-polymer blends are promising materials for organic photovoltaics, with light absorption in both components. Initially all-polymer cells made with blends of poly(dialkoxy-*p*-phenylene vinylene) (PPV) derivatives have performed poorly [4, 5]. However, recently the efficiencies of devices based on PPV-derivatives as a donor have been strongly increased [6, 7], starting to approach the 2.5% of PPV derivatives when blended with fullerenes [8]. For blends of MDMO-PPV and PCNEPV morphology studies show a strong intermixing of the two polymer phases with the size of the polymer domains formed in the blend not far from the exciton diffusion length [5]. Though having a large open circuit voltage (V_{oc}), the efficiency of an optimized device, including an additional acceptor top layer and thermal treatment, was lower than 1% [5]. However, the reason for the relatively poor performance of these devices, especially the unannealed ones, as compared to their fullerene counterparts is not clear. One of the main reasons for the relatively low efficiencies is the fact that the fill factor (FF) is less than 25%, i.e., about twice as low as for MDMO-PPV:PCBM devices. In earlier work on fullerene devices it was demonstrated that under reverse bias the shape of the photocurrent versus voltage is strongly dependent on the generation efficiency of free carriers from bound electron-hole pairs [9]. The electric field and temperature dependence of the photocurrent can be described with a model based on Onsager's theory of geminate charge recombination. Furthermore, strongly unbalanced transport leads to the formation of space-charge in the solar cell [10]. The resulting square-root dependence of the photocurrent on voltage also strongly reduces the FF of space-charge limited devices. In the previous chapter, the charge transport properties of MDMO-PPV:PCNEPV blends (1:1 wt.%) have been investigated. The hole transport in the MDMO-PPV phase is space-charge limited and the hole mobility is equal to the value of the pristine polymer, being 5×10^{-10} m^2/Vs at room temperature. The electron transport in the PCNEPV phase is, however, strongly trap-limited [11]. The presence of electron traps leads to a highly unbalanced charge transport in this type of blends. In this chapter we address the possible causes of the low FF and resulting poor efficiency, and show the limiting mechanisms that must be overcome for future efficient all-polymer solar cells.

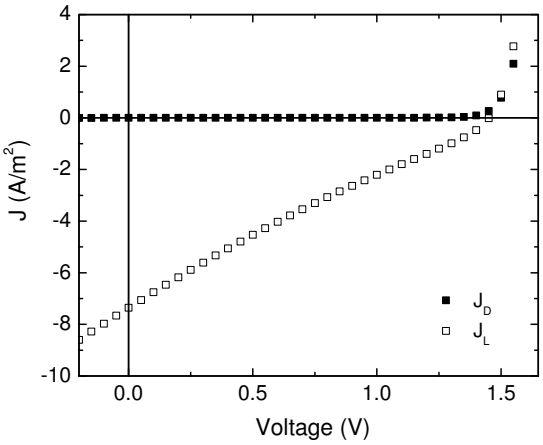

Figure 5.1: Typical dark (solid symbols) and illuminated (open symbols) J-V characteristics of a MDMO-PPV:PCNEPV solar cell. The device was illuminated with 1000 W/m^2 white light.

5.2 The photocurrent of MDMO-PPV:PCNEPV solar cells

In all-polymer bulk heterojunction (BHJ) solar cells, an exciton generated in the donor and/or acceptor phase can diffuse towards the interface between the two polymers. Subsequently, electron transfer to the acceptor (hole transfer to the donor) occurs due to the difference in the electron affinities and ionization potentials of the two polymers. In this way, a bound electron-hole (e-h) pair is formed across the interface, with the hole in the donor polymer and the electron in the acceptor polymer. Due to the low dielectric constants ε_r of the organic materials (ε_r ranges typically from 2 to 4), these e-h pairs are strongly bound by Coulomb interaction, with binding energies of typically several tenths of an electron volt. This bound pair still needs to dissociate with the help of the internal electric field in the device in order to produce free carriers, which are then transported to the appropriate electrodes. In Figure 5.1, the J-V characteristics measured in the dark (J_D) and under illumination (J_L) with 1000 W/m^2 white light are shown for a typical MDMO-PPV:PCNEPV (1:1 wt. ratio) solar cell, with an active layer thickness of 50 nm. The current under illumination is almost linear, with an apparent inward bend, resulting in a low fill factor.

As a result, the high open-circuit voltage of MDMO-PPV:PCNEPV solar cells

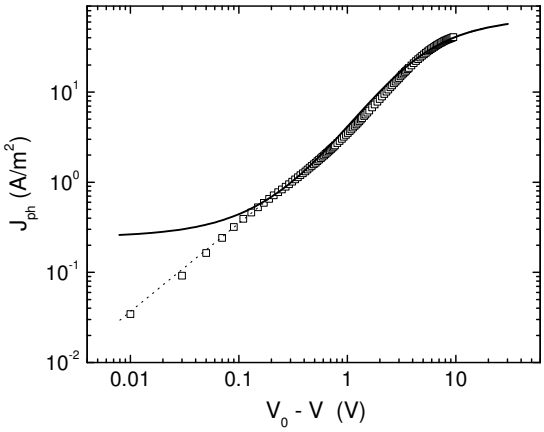

Figure 5.2: Photocurrent versus effective applied voltage (symbols) of a typical MDMO-PPV:PCNEPV solar cell, with an active layer thickness of 50 nm. The dotted line is a guide to the eye, showing the dependence on voltage with the slope of 1. The solid line is given by $J = eG(E,T)L$ with $G(E,T)$ containing the calculated dissociation efficiency in this case.

is counterbalanced by the low short-circuit current and the low fill factor, leading to poor efficiencies. To study the dependence of the photocurrent on electric field we have plotted in Figure 5.2 the photocurrent ($J_{ph} = J_L - J_D$) of a typical MDMO-PPV:PCNEPV solar cell, against the effective applied voltage ($V_0 - V$), where V_0 is the compensation voltage, which is defined as the voltage for which the photocurrent J_{ph} is zero [9]. In MDMO-PPV:PCBM (1:4 wt. ratio) solar cells, the photocurrent linearly increases with voltage at a voltage close to the compensation voltage V_0 ($V_0 - V < 0.1$ V) due to a competition between drift and diffusion currents. For $V_0 - V > 0.1$ V the photocurrent enters the saturation regime where it can be approximated by $J_{ph} = eG(E,T)L$, with e the elementary charge, $G(E,T)$ the generation rate of free carriers, and L the sample thickness [9]. The rate $G(E,T)$ is governed by the dissociation efficiency of the bound e-h pairs, which is a field- and temperature dependent process.

As shown in Figure 5.2, also in the MDMO-PPV:PCNEPV solar cells these two regimes occur: A linear regime for $V_0 - V < 0.1$ V (dotted line), where carrier drift and diffusion compete, followed by a S-shape like regime (solid line) for $V_0 - V > 0.1$ V. Such an S-shape of the photocurrent versus effective voltage is characteristic

for the field-dependent dissociation process of the bound *e-h* pairs; at low (or zero) field there is still dissociation of bound pairs taking place via thermal excitation (as also evident from Equation 5.3 when $b \to 0$). However, compared to the MDMO-PPV:PCBM cells, the dissociation efficiency at low effective voltages in the all-polymer MDMO-PPV:PCNEPV cells is much lower. In MDMO-PPV:PCBM the difference between the dissociation at low fields ($V_0 - V \sim 0.1$ V) and at full saturation at high fields ($V_0 - V \sim 10$ V) is typically a factor 3, meaning that $1/3^{rd}$ of the bound *e-h* pairs is already dissociated at low fields. From Figure 5.2 it appears that the difference in the all-polymer cell is much larger, and typically amounts to two orders of magnitude. So only a small fraction of the created *e-h* pairs actually contributes to the photocurrent at low voltages. It is evident that such a low dissociation efficiency will be responsible for a strongly reduced photocurrent. Furthermore, its strong field dependence and the resulting inward bend in the fourth quadrant (Figure 5.2) strongly suppresses the fill factor. The major question now is why the dissociation is so poor in these all-polymer solar cells.

5.3 Dissociation efficiency

Due to the strong Coulomb binding energy in organic solar cells, only a certain fraction of all the photo-generated bound electron-hole pairs G_{max} is dissociated into free charge carriers, depending on field and temperature, and therefore contributes to the photocurrent (eGL). Consequently, the generation rate G of free charge carriers can be described by

$$G(T, E) = G_{max} P(T, E), \tag{5.1}$$

where $P(T, E)$ is the probability for charge separation at donor/acceptor interface. As stated above, the photogeneration of free charge carriers in low-mobility materials can be explained by the geminate recombination theory of Onsager [12]. An important addition to the theory has been made by Braun [13], who stressed the importance of the fact that the bound electron-hole pair (or charge transfer state) has a finite lifetime. In Braun's model, the probability that a bound polaron pair dissociates into free charge carries at a given electric field E and temperature T is given by

$$P(T, E) = \frac{k_D(E)}{k_D(E) + k_F}, \tag{5.2}$$

with k_F the rate constant that the bound electron-hole pair decays to its ground state, and $k_D(E)$ the rate constant for separation into free carriers, which is given

by [13]

$$k_D(E) = k_R \frac{3}{4\pi a^3} e^{-E_B/kT} \left[1 + b + \frac{b^2}{3} + \frac{b^3}{18} + \frac{b^4}{180}\right], \tag{5.3}$$

with a the initial separation distance of the bound electron-hole pair at the interface, $b = e^3E/8\pi\varepsilon_0\varepsilon_r k^2T^2$, and E_b the binding energy of the electron-hole pair.

Once separated, the charge carriers can again form a bound pair with a rate constant k_R. The dissociation model uses the Onsager theory for field-dependent dissociation rate constants for weak electrolytes [12] for $k_D(E)$, Langevin recombination of free electrons and holes and a Gaussian distribution of donor-acceptor distances. Then, the generation rate of producing free electrons and holes depends on the charge carrier mobilities μ_n and μ_p of the electron and holes respectively, the relative dielectric constant ε_r, the initial separation of e-h pairs a, and the ground state recombination rate k_F. As a next step we investigate the relevance of these parameters for the dissociation in the MDMO-PPV:PCNEPV all-polymer cells. In Figure 5.3 the dissociation probability $P(E,T)$ is shown for a MDMO-PPV:PCBM (1:4 wt. ratio) based solar cell (solid line). For this system, an initial electron-hole pair separation distance $a = 1.3$ nm, a decay rate $k_F = 1.0 \times 10^5$ s^{-1}, a dielectric constant $\varepsilon_r = 3.4$, and electron and hole mobilities of $\mu_n = 2.0 \times 10^{-7}$ m^2/Vs and $\mu_p = 2.0 \times 10^{-8}$ m^2/Vs have been used to describe the experiments [14]. As shown in *Chapter 4* on the charge transport properties of MDMO-PPV:PCNEPV (1:1 wt. ratio) mobilities of $\mu_n = 6.0 \times 10^{-11}$ m^2/Vs and $\mu_p = 5.0 \times 10^{-10}$ m^2/Vs have been measured [11]. As a first step we now include these lower mobility values into the calculation of $P(E,T)$, leaving all the other parameters equal to the MDMO-PPV:PCBM case (dashed line). At $V_0 - V = 0.1$ V the dissociation probability now decreases from 2.6×10^{-1} to 2.8×10^{-3} due to the reduced mobilities in the all-polymer system. A beneficial effect for the dissociation in MDMO-PPV:PCBM cells was that with increasing PCBM content also the spatial average dielectric constant $< \varepsilon_r >$ of the blend was increasing, since the ε_r of 4.0 of PCBM is significantly larger than the 2.1 of MDMO-PPV [14]. At a 1:4 wt. ratio this resulted in an average $< \varepsilon_r >$ of 3.4. For the pristine PCNEPV we determined an ε_r of 3.2 from impedance measurements. In a 1:1 weight ratio of PCNEPV and MDMO-PPV in the blend, this results in an average $< \varepsilon_r >$ of 2.6. The dotted line in Figure 5.3 shows the calculated dissociation probability $P(E,T)$ with the reduced mobilities and also the reduced $< \varepsilon_r >$ included. As a result, at $V_0 - V = 0.1$ V, $P(E,T)$ further decreases to 5.28×10^{-4}, which lowers the photocurrent to values even below the experimentally observed one. As a final step we also modify the dissociation parameters a and k_F (dashed-dotted line). Using $k_F = 1 \times 10^2$ s^{-1} and $a = 0.6$ nm, a good agreement with the experiment is obtained.

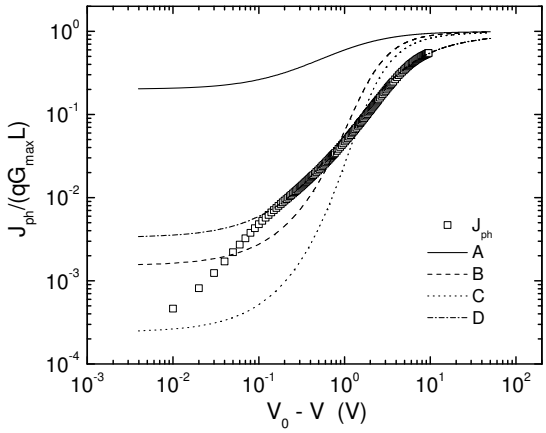

Figure 5.3: (A) Calculated dissociation efficiency $P(E,T)$ for a MDMO-PPV:PCBM solar cell (solid line), with a maximum generation rate $G_{max} = 2.7 \times 10^{27}$ m^{-3}s^{-1}, an initial electron-hole pair separation distance $a = 1.3$ nm, a decay rate $k_F = 1.0 \times 10^5$ s^{-1}, a relative dielectric constant $\varepsilon_r = 3.4$, and constant electron and hole mobilities $\mu_n = 2.0 \times 10^{-7}$ m^2/Vs and $\mu_p = 2.0 \times 10^{-8}$ m^2/Vs. (B) The dashed line is the calculation for the same generation parameters, only the carrier mobilities are equal to the ones of the MDMO-PCNEPV system, $\mu_n = 6.0 \times 10^{-11}$ m^2/Vs and $\mu_p = 5.0 \times 10^{-10}$ m^2/Vs. (C) The dotted line is the calculation for the latter case, with also the spatial average dielectric constant of the polymeric system, $< \varepsilon_r >= 2.6$ included. (D) The dashed-dotted line shows $P(E,T)$ for the all-polymer system using $k_F = 1.0 \times 10^2$ s^{-1} and $a = 0.6$ nm. The active layer has been assumed for all cases to be 50 nm. The symbols are the experimental MDMO-PPV:PCNEPV solar cell photocurrent, for an active layer of 50 nm.

Compared to the MDMO-PPV:PCBM blend, the separation distance between the bound *e*-*h* pair has been strongly reduced, together with a decrease of its decay rate. This indicates that in the all-polymer blend the electron-hole pairs are strongly bound with a small separation distance, and a small decay rate, meaning a long lived charge transfer state. It is evident that a small separation distance will lead to a reduced dissociation efficiency, since the Coulomb binding energy will strongly increase. For polymeric heterojunctions based on polyfluorenes it

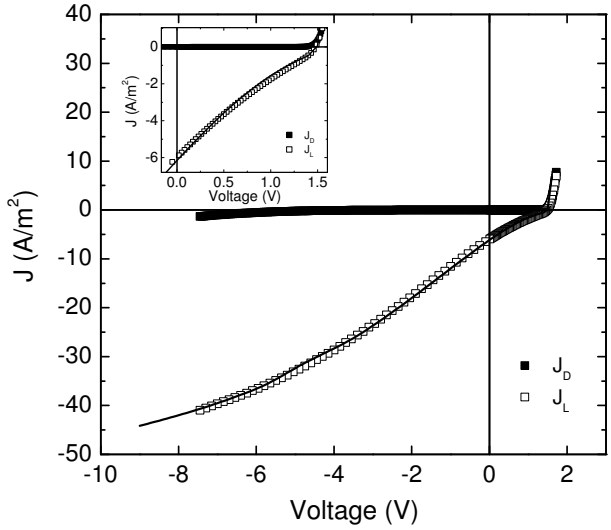

Figure 5.4: Dark (solid symbols) and illuminated (open symbols) characteristics of a MDMO-PPV: PCNEPV solar cell, with an active layer of 50 nm. The solid line is the calculated current with a maximum generation rate $G_{max} = 9.3 \times 10^{27}$ m^{-3}s^{-1}, an electron-hole pair distance $a = 0.62$ nm, a decay rate $k_F = 7.0 \times 10^2$ s^{-1} and carrier mobilities derived from transport measurements, with $\mu_p = 5.0 \times 10^{-10}$ m^2/Vs, $\mu_n = 6.0 \times 10^{-11}$ m^2/Vs, and the electron trapping parameters $N_t = 9.6 \times 10^{22}$ and $T_t = 2500$ K. The inset shows the magnified fourth quadrant of the J-V.

is known that exciplexes are formed, indicative of a strong coupling between the electron and hole [15]. On the other hand, a strong coupling between the bound electron and hole is also expected to increase their recombination rate k_F. This increased recombination is in contrast with the small recombination rate that we obtain. An explanation might be that excitons are regenerated at these heterojunctions because due to its long lifetime the exciplex can be back transferred into the bulk as an exciton [15]. Subsequently, part of these regenerated bulk excitons will be dissociated again at the heterojunction, and again appear as bound pairs. In our dissociation model such an effect will show up as an increase of the effective lifetime of the bound pair. From photophysical studies on the MDMO-PPV:PCNEPV blend also exciplex formation was found by Offermans *et al.*; this formation was in competition with the formation of free charge carriers, which can

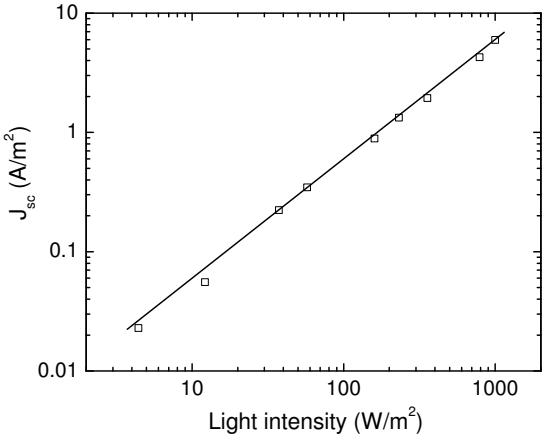

Figure 5.5: The dependence of the short-circuit current J_{sc} on the light intensity of a typical MDMO-PPV:PCNEPV solar cell (symbols) for an active layer of 50 nm. The solid line has a slope 1, showing the linear dependence of J_{sc} on the light intensity.

be described by the dissociation efficiency defined by Equation 5.2 [16]. Probably, the small separation distance between the bound e-h pair in these all-polymer blends originates from the morphology of these films. In MDMO-PPV:PCBM (1:4 wt. ratio) films, PCBM is known to form crystallites [17], which might enhance the delocalization of the electrons. This would translate in a larger initial separation distance between the electrons and holes. In the MDMO-PPV:PCNEPV blends the phase separation is not as pronounced and the morphology is closer to a full intermixing on the molecular scale [5], leading to smaller separation distances between the bound e-h pair.

5.4 The photocurrent-numerical results

5.4.1 Langevin recombination

In order to model the photocurrent of MDMO:PCNEPV solar cells we use a device model [18] that includes drift and diffusion, the field- and temperature dependent generation rate $G(E,T)$, and the carrier mobilities and trapping parameters as obtained from recent measurements [11]. In Figure 5.4 the measured and simulated photocurrents are shown. Since the simulations take into account that the electric field and the coupled generation rate are not completely homogeneous,

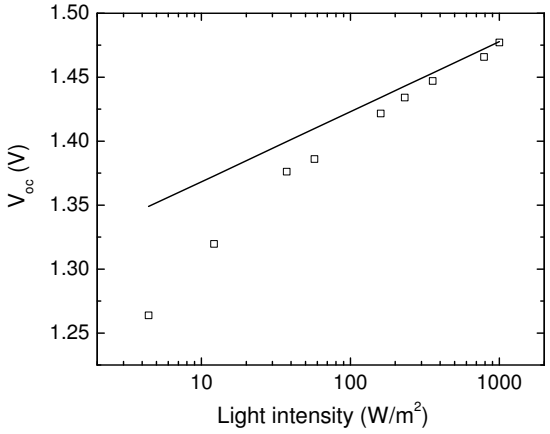

Figure 5.6: Experimental open-circuit voltage (V_{oc}) of a typical MDMO-PPV:PCNEPV cell (symbols), with an active layer of 50 nm, and the calculation (line), with the parameters used to calculate the J-V characteristic, in case of Langevin recombination.

the dissociation parameters a and k_F have to be slightly adapted as compared to Figure 5.3 to get the best fit.

The good agreement shows that the photocurrent of these all-polymer cells can be described within the same framework as the MDMO-PPV:PCBM cells. The major difference is the much smaller dissociation efficiency at low fields, also resulting in a steeper field-dependence at higher voltage. It should also be noted that the total amount of photogenerated e-h pairs $G_{max} = 9.3 \times 10^{27}$ m^{-3}s^{-1}, as obtained from the saturated photocurrent at high reverse bias, is considerably larger as compared to the MDMO-PPV:PCBM based counterparts, where $G_{max} = 2.5 \times 10^{27}$ m^{-3}s^{-1} had been found [14]. Clearly, the all-polymer cells absorb more light, but the problem is to get the photogenerated electrons and holes separated. From the voltage dependence of the photocurrent, no space charge effects seem to be present, their signature being a much lower dependence on voltage, with a slope of 0.5. This voltage dependence stems from the fact that in case of carrier accumulation $J_{ph} = eG(E,T)d$, where d is the width accumulation region that is voltage dependent. To further verify that for $V_0 - V > 1$ V the photocurrent is saturated and can be approximated by $J_{ph} = eG(E,T)L$, we also investigated the intensity dependence of the short-circuit current J_{sc}. In Figure 5.5, the measured short-circuit current is plotted as function of light intensity. The linear behavior obtained, as expected from $eG(E,T)L$, also shows that

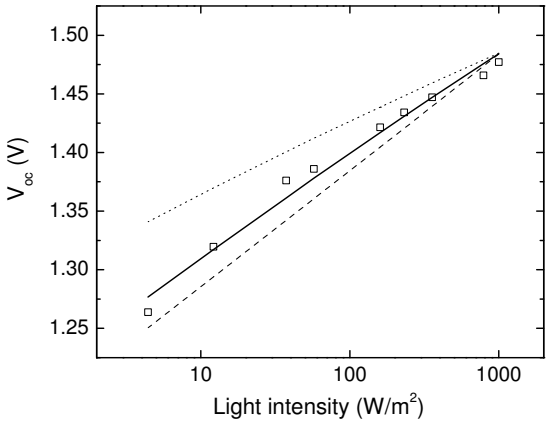

Figure 5.7: V_{oc} versus light intensity (symbols) of a typical MDMO-PPV:PCNEPV solar cell, with an active layer of 50 nm, and the calculated lines using the mobility values derived from transport measurements, and the capture coefficients for electrons and holes $C_n = C_p = 1.4 \times 10^{-18}$ m^{3}s^{-1} (solid line), $C_n = C_p = 5.0 \times 10^{-20}$ m^{3}s^{-1} (dotted line) and $C_n = C_p = 5.0 \times 10^{-17}$ m^{3}s^{-1} (dashed line).

space-charge effects, which would give a slope of 0.75, do not play a role at short circuit in these devices. This is also expected since due to the low dissociation efficiency there are only a limited amount of free carriers available to create space charge.

As a last step we also investigate the intensity dependence of the open-circuit voltage V_{oc}. It has been shown that in case of Langevin recombination, the open-circuit voltage V_{oc} of a solar cell depends linearly with the logarithm of the light intensity, with a slope kT/q [19]. This was experimentally verified on various PPV-based fullerene systems. However, for the MDMO-PPV:PCNEPV solar cells, as shown in Figure 5.6, the experimental data show a much steeper slope, whereas the calculated open-circuit voltage from the numerical device model with the parameters mentioned above has the expected kT/q slope.

5.4.2 Langevin and trap-assisted recombination

Apparently, in our model of the all-polymer cells there is still a process missing. At open-circuit there is no current extraction and all the photogenerated charge carriers recombine [18]. As a result, the properties of the solar cell at open-circuit

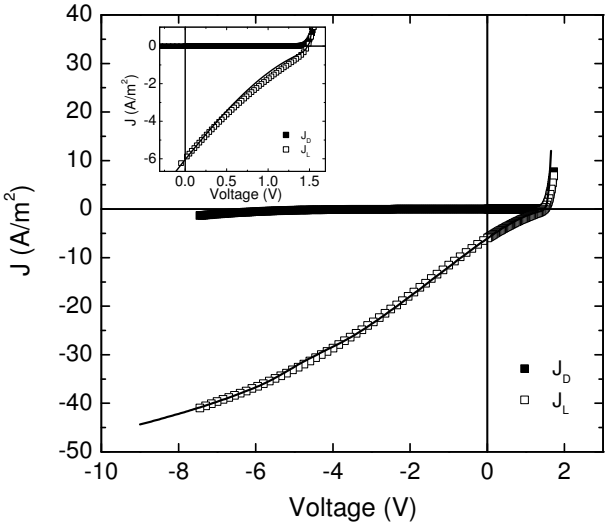

Figure 5.8: Dark (solid symbols) and illuminated (open symbols) J-V characteristics of a MDMO-PPV:PCNEPV solar cell, with an active layer of 50 nm. The solid line is the calculated current with a maximum generation rate $G_{max} = 9.4 \times 10^{27}$ m^{-3}s^{-1}, an electron-hole pair distance $a = 0.62$ nm, a decay rate $k_F = 6.7 \times 10^2$ s^{-1} and carrier mobilities derived from transport measurements, with $\mu_p = 5.0 \times 10^{-10}$ m^2/Vs, $\mu_n = 6.0 \times 10^{-11}$ m^2/Vs, the electron trapping parameters $N_t = 9.6 \times 10^{22}$ and $T_t = 2500$ K, and the capture coefficients $C_n = C_p = 1.4 \times 10^{-18}$ m^{3}s^{-1}. The inset shows the magnified fourth quadrant of the J-V.

are strongly dependent on the recombination processes. In the previous chapter we demonstrated that the electron transport in PCNEPV phase is strongly trap-limited [11]. In such a case, electrons get immobilized in the traps, and can, subsequently, recombine with free holes. Such a trap-assisted recombination path has not been included in the device model so far, because in the earlier studies on PPV-fullerene cells the electron and hole transport can be regarded as trap-free. The trap-assisted recombination is described by the Shockley-Read-Hall (SRH) equation [20, 21] for which the recombination rate is given by [22]

$$R = C_n C_p N_t (pn - p_1 n_1)/[C_n(n + n_1) + C_p(p + p_1)], \tag{5.4}$$

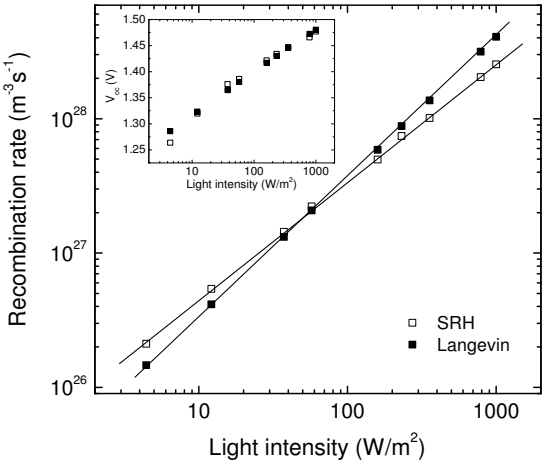

Figure 5.9: Rate of trap-assisted recombination (open symbols) and of Langevin recombination (solid symbols), as function of light intensity, for the parameters used to calculate the current under illumination at 1000 W/m^2, with a field-dependent generation rate G. The solid lines are a guide for the eye. The inset shows the light intensity dependence of the measured V_{oc} (open symbols) and the calculated values (solid symbols), corresponding to the calculated recombination rates.

where C_n, C_p are the capture coefficients of electrons and of holes, respectively, N_t is the density of electron traps, n and p are the electron density in the conduction band and the hole density in valence band, and $p_1 n_1 = N_c N_v \exp[-(E_c - E_v)/kT] = n_i^2$, which is the intrinsic carrier concentration in the sample. In Figure 5.7 we show the influence of the C_n and C_p, which are assumed to be equal (every trapped electron can capture a free hole), on the light-intensity dependence of the V_{oc}. Using $C_n = C_p = 1.4 \times 10^{-18}$ m^{3}s^{-1}, the light-intensity dependence of the V_{oc} is in agreement with the experiments. In this case, both Langevin and Shockley-Read-Hall recombination play a role in the solar cell.

Including the trap-assisted recombination in the device model we recalculate the photocurrent of the MDMO-PPV:PCNEPV all-polymer cell as shown in Figure 5.8. The dissociation parameters are not affected by the inclusion of the SRH recombination. As stated above, recombination is especially important at open-circuit. However, at short-circuit and in reverse bias almost all electrons and holes are extracted and recombination losses become negligible.

For the understanding of the device operation it is important to know which

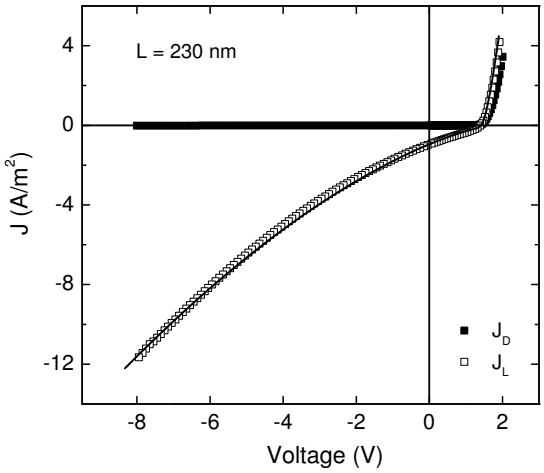

Figure 5.10: Dark (solid symbols) and illuminated (open symbols) J-V characteristics of a MDMO-PPV: PCNEPV solar cell, with an active layer of 230 nm. The solid line is the calculated current with a maximum generation rate $G_{max} = 3.5 \times 10^{27}$ m^{-3}s^{-1}, an electron-hole pair distance $a = 0.62$ nm, a decay rate $k_F = 6.7 \times 10^2$ s^{-1} and carrier mobilities derived from transport measurements, with $\mu_p = 5.0 \times 10^{-10}$ m^2/Vs, $\mu_n = 6.0 \times 10^{-11}$ m^2/Vs, the electron trapping parameters $N_t = 9.6 \times 10^{22}$ and $T_t = 2500$ K, and the capture coefficients $C_n = C_p = 1.4 \times 10^{-18}$ m^{3}s^{-1}.

recombination mechanism is responsible for the losses in the solar cell. As shown in Figure 5.9 the strength of the Langevin recombination is clearly dominant compared to the trap-limited SRH recombination at 1000 W/m^2. This is another reason why the inclusion of SRH recombination does not strongly affect the calculated photocurrent shown in Figure 5.4, where only Langevin recombination was taken into account. At lower light intensities (< 100 W/m^2), the trap-assisted recombination takes over from the Langevin recombination since it has a weaker dependence on carrier density.

Thus, trapping effects are important at the open-circuit voltage, but have only limited influence on the J-V characteristics at normal and high light intensities. The assumption of a strongly bound electron-hole pair is necessary in both cases (trap assisted recombination or not) in order to model the current under illumination.

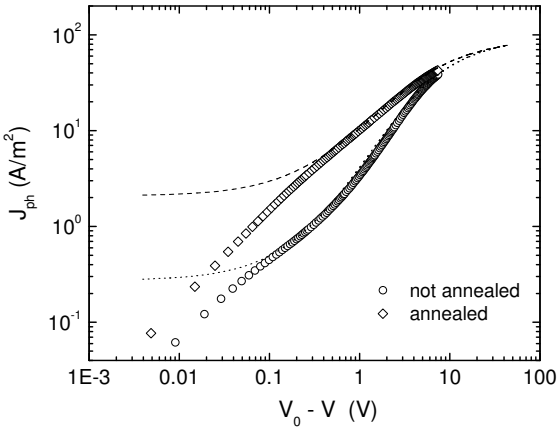

Figure 5.11: The photocurrent versus the applied voltage for MDMO-PPV:PCNEPV solar cells, without thermal treatment (circles) and annealed at 120 °C for 15 minutes (diamonds). The thickness of the active layer is in both cases around 40 nm. The dash and dotted line are a guide to the eye.

We checked the validity of our model on a much thicker device, of 230 nm, as it can be seen in Figure 5.10. The photocurrent can be modeled with all the parameters kept the same. The only correction made is for the maximum generation rate G_{max}, which for thicker samples has a lower rate since it represents an average value over sample thickness. In this case the rate amounts to 3.5×10^{27} m^{-3}s^{-1}. Trap-assisted recombination has been included as well, with the same value for the capture coefficients as for the thin device of 50 nm.

5.5 Efficiency improvement in MDMO:PCNEPV solar cells

The efficiency of this type of solar cells can be further increased by a thermal treatment: annealing at 120 °C for ten minutes leads to an efficiency increase from 0.25% to 0.5%. Adding another acceptor layer increases the efficiency even further towards 0.75%, as has been shown in Reference 5. For the unannealed devices we have shown that the low FF and performance originates from a low dissociation efficiency. This poor dissociation is a combined effect of the low mobility, low dielectric constant, and the small separation distance between electrons

and holes (related to the morphology). As can be seen from Figure 5.11 annealing strongly changes the shape of the photocurrent. At high bias the photocurrents coincide, showing that the amount of photogenerated *e-h* pairs has not changed. The change of the *S*-shape like form indicates that annealing improves the dissociation efficiency in this type of cells. However, it is not clear what is the main mechanism through which this improvement is done: an increase in mobility, due to a better transport after annealing, a change in the dielectric constant or a change in morphology upon annealing, facilitating the dissociation. This subject is further investigated in *Chapter 7* of this thesis.

5.6 Conclusion

We have investigated the photogeneration and recombination of charges in blends of all-polymer BHJ solar cells based on MDMO-PPV:PCNEPV. The electron traps present in the PCNEPV phase contribute to the recombination losses of the system at low light intensities. The trap-assisted recombination dominates the superlinear light intensity dependence of the open-circuit voltage observed for this type of solar cells. However, at a light intensity of 1 Sun, the Langevin recombination is the main loss mechanism, dominating over the trap-assisted recombination. The photogenerated current is dominated by the poor dissociation efficiency of a strongly bound, long-lived electron-hole pair. The combination of low carrier mobilities, low dielectric constant and morphology gives rise to strongly field-dependent photogeneration efficiency, which explains the low photocurrents at operating voltages in the fourth quadrant, as well as the strongly reduced fill factor.

5.7 Experimental

The electron donor MDMO-PPV was synthesized using the sulfinyl route [23], yielding a molecular weight of 300 kg/mol and a polydispersity index of 2.7. As electron acceptor, PCNEPV was synthesized as described elsewhere [24], with a molecular weight of 73.4 kg/mol and a polydispersity index of 3.3. The molecular weights and polydispersity indexes were measured against poly(styrene) standards. Both polymers were synthesized at TNO. The solar cells were prepared on ITO-coated glass substrates, provided by Philips Research. All substrates were cleaned, dried and treated with UV-ozone prior to PEDOT:PSS (Bayer AG) spin-coating. After spin-coating, the PEDOT:PSS layer was dried at 140 °C for 10 minutes, and, subsequently, the polymer blend was spin-coated from chlorobenzene solution in a nitrogen atmosphere. Subsequently, 1 nm of LiF, followed by

100 nm Al, was deposited by thermal evaporation as top electrode at a chamber pressure of $\sim 10^{-6}$ mbar. The annealing of the devices was performed in a N_2 atmosphere, on a hot plate at 120 °C, for 15 minutes, before the deposition of the top electrode. The devices were characterized using a Keithley 2400 SourceMeter, the measurements being performed under nitrogen atmosphere. To measure the illuminated characteristics (J_L), the solar cells have been illuminated through the ITO electrode with a white light tungsten-halogen lamp, for which the intensity has been set using a calibrated Si diode.

References

[1] W. Ma, C. Yang, X. Gong, K. Lee, and A.J. Heeger, Adv. Funct. Mater. **15**, 1617 (2005).

[2] G. Li, V. Shrotriya, J. Huang, Y. Yao, T. Moriarty, K. Emery, and Y. Yang, Nature Mater. **4**, 864 (2005).

[3] M. Reyes-Reyes, K. Kim, and D. L. Carroll, Appl. Phys. Lett. **87**, 083506 (2005).

[4] J. J. M. Halls, C. A. Walsh, N. C. Greenham, E. A. Marseglia, R. H. Friend, S. C. Moratti, and A. B. Holmes, Nature **376**, 498 (1995).

[5] S. C. Veenstra, W. J. H. Verhees, J. M. Kroon, M. M. Koetse, J. Sweelssen, J. J. A. M. Bastiaansen, H. F. M. Schoo, X. Yang, A. Alexeev, J. Loos, U. S. Schubert, and M. M. Wienk, Chem. Mater. **16**, 2503 (2004).

[6] M. M. Koetse, J. Sweelssen, K. T. Hoekerd, H. F. M. Schoo, S. C. Veenstra, J. M. Kroon, X. Yang, and J. Loos, Appl. Phys. Lett. **88**, 083504 (2006).

[7] T. Kietzke, H.-H. Hörhold, and D. Neher, Chem. Mater. **17**, 6532 (2005).

[8] S. E. Shaheen, C. J. Brabec, N. S. Sariciftci, F. Padinger, T. Fromherz, and J. C. Hummelen, Appl. Phys. Lett. **78**, , 841 (2001).

[9] V. D. Mihailetchi, L. J. A. Koster, J. C. Hummelen, and P. W. M. Blom, Phys. Rev. Lett. **93**, 216601 (2004).

[10] V. D. Mihailetchi, J. Wildeman, and P. W. M. Blom, Phys. Rev. Lett. **94**, 126602 (2005).

[11] M. M. Mandoc, W. Veurman, L. J. A. Koster, M. M. Koetse, J. Sweelssen, B. de Boer and P. W. M. Blom, J. Appl. Phys. **101**, 104512 (2007).

[12] L. Onsager, J. Chem. Phys. **2**, 599 (1934).

[13] C. L. Braun, J. Chem. Phys. **80**, 4157 (1984).

[14] V. D. Mihailetchi, L. J. A. Koster, P. W. M. Blom, C. Melzer, B. de Boer, J. K. J. van Duren, and R. A. J. Janssen, Adv. Funct. Mater. **15**, 795 (2005).

[15] A. C. Morteani, P. Sreearunothai, L. M. Herz, R. H. Friend, and C. Silva, Phys. Rev. Lett. **92**, 247402 (2004).

[16] T. Offermans, P. A. van Hal, S. C. J. Meskers, M. M. Koetse, and R. A. J. Janssen, Phys. Rev. B **72**, 045213 (2005).

[17] J. K. J. van Duren, X. Yang, J. Loos, C. W. T. Bulle-Lieuwma, A. B. Sieval, J. C. Hummelen, and R. A. J. Janssen, Adv. Funct. Mater. **14**, 425 (2004).

[18] L. J. A. Koster, E. C. P. Smits, V. D. Mihailetchi, and P. W. M. Blom, Phys. Rev. B **72**, 085205 (2005).

[19] L. J. A. Koster, V. D. Mihailetchi, R. Ramaker, and P. W. M. Blom, Appl. Phys. Lett. **86**, 123509 (2005).

[20] W. Shockley, and W. T. Read, Phys. Rev. 87, 835 (1952).

[21]] R.N. Hall, Phys. Rev. **87**, 387 (1952).

[22] K. C. Kao, W. Hwang, *Electrical transport in solids*, Pergamon Press, Oxford, 1981.

[23] L. Lutsen, P. Adriaensens, H. Becker, A. J. van Breemen, D. Vanderzande, and J. Gelan, Macromolecules **32**, 6517 (1999).

[24] M. M. Koetse, J. Sweelssen, T. Franse, S. C. Veenstra, J. M. Kroon, X. Yang, A. Alexeev, J. Loos, U. S. Schubert, and H. F. M. Schoo, Proc. SPIE-Int. Soc. Opt. Eng.**5215**, 119 (2004).